Composite Structures 121 (2015) 172–181

Contents lists available at ScienceDirect

Composite Structures

journal homepage: www.elsevier.com/locate/compstruct

Impact response of thick composite plates under uniaxial tensile preloading

N. Guillaud [a,*], C. Froustey [b], F. Dau [a], P. Viot [a]

[a] Arts et Métiers Paristech, Institut de Mécanique et d'Ingénierie de Bordeaux, UMR CNRS 5295, Esplanade des Arts et Métiers, F-33400 Talence, France
[b] Université de Bordeaux, Institut de Mécanique et d'Ingénierie de Bordeaux, UMR CNRS 5295, Esplanade des Arts et Métiers, F-33400 Talence, France

ARTICLE INFO

Article history:
Available online 13 November 2014

Keywords:
Composites
Carbon fibers
Low-velocity impact
Preloading
Thick plate

ABSTRACT

This work focuses on the impact response of composite plates 5 mm thick subjected to uniaxial tension preload. Laminated carbon/epoxy with quasi-isotropic stacking sequence $([0/45/90/-45]_2)_S$ samples were used. Doehlert-type design of experiments was proposed to investigate the influence of both preload and impact energy on impact composite responses. Deformation, varying from 300 to 3000 micro-strain, was imposed thanks to a preload device designed for this purpose. Impacts were generated using a home made drop tower. Imposed impact energy was varying from 30 to 214 J. Post-impact damage was characterized by both non-destructive (ultrasound) and destructive (deply) techniques. Influence of the preloading on delamination areas (total and projected) was quantified and found sensitive to the preloading.

1. Introduction

Composite materials are increasingly used in aerospace due to their high stiffness to mass ratio compared to other materials. These materials are known for their vulnerability to low-velocity impact from foreign objects [1–3], such as drop of tools during maintenance for example. Low velocity impact produce internal defects in the form of delaminations and matrix breaking which are difficult to be detected from routine inspection like visual inspection. This type of damages can significantly reduce the residual strength and stiffness of the material, as a consequence they are considered critical for the structures. Impact behavior of composites has been extensively treated in the literature. The state of the art is related in a lot of overviews [4–8]. Nevertheless, most of these investigations focus on composite laminates that are unloaded during impact and generally concern thin structures. A major challenge now is to use composite materials as structural parts. These materials are usually responsible of carrying large loads, either in operation or at rest, and may in some cases have very large thickness. There is a strong interest in investigating the influence of preloads on the impact response of thick composite structures.

In the literature, few studies deal with the impact behavior of preloaded plates or shells [9]. Usually, imposed preloading amount to 6000 με for the glass fiber reinforced polyester (GFRP) [10,9] and to 2500 με for carbon fiber reinforced polyester (CFRP) [11]. The influence of uniaxial preload on the response on impact damage is reported in references [12,13,11]. In these references, low velocity impact on quasi-isotropic CFRP [12,11] and GFRP [13] plates have been studied and concern thin plates. Uniaxial preload was imposed by hydraulic actuator and vary from 500 με to 2400 με. It was observed that the damaged area and the contact force increased with a tensile preload [12,11]. On the contrary, Mitrevski et al. [13] observed that preload altered the indentation depth (for conical impactor) and did not modify the damaged area.

Saghafi et al. [9], induced compressive uniaxial preload on thin curved panels. In this work, two boundary conditions were tested, free and guided lateral edge. They showed that when the preload increase, the damaged area was higher.

The influence of a biaxial preload is studied in [13,10,14]. The results show that tension/tension biaxial preloads rise the contact force peak for GFRP, while CFRP is found insensitive to preload for at least low energy (less than 10 J) and low preload (less than 1500 με). Robb et al. [10] performed low-velocity impact tests on GFRP laminated plates. These plates were impacted at the energy of 21.5 J with preload in biaxial tension, biaxial compression and tension compression (±2000 με, ±4000 με, ±6000 με). They showed that the absorbed energy was lowest for a tension/tension configuration. Ghelli and Minak [15] worked on numerical analysis of the effect of membrane preloads on the low-speed impact response of composite laminates. They proved that a uniaxial ten-

* Corresponding author.

http://dx.doi.org/10.1016/j.compstruct.2014.11.021
0263-8223/

sile preloads increase the peak stresses and this effect was stronger for biaxial preloads.

Kulkarni et al. [16] induced biaxial preloading imposing air pressure on one face of the plate. They showed little preload influence on contact force, which was justified by the effect of the plate curvature induced by pressure. The decrease of contact force due to curvature was previously observed in [17].

Heimbs et al. [18] studied the impact resistance of preloaded composite plate during a hight velocity impact. Carbon/epoxy samples were preloaded in compression and in tension. The experimental tests prove that the damaged area was reduced for tension preloading. Absorbed energy was higher for tension preloaded case than unpreloaded. Garcia-Castillo et al. [19,20] worked on the hight velocity impact resistance of preloaded carbon composite plates. They proved that the ballistic limit was higher and the damage area was lower for biaxial loading than for unpreloaded samples. The maximum impact energy supported by biaxial preloaded samples was 11% higher.

The present work is a part of a research program about the impact behavior of thick preloaded composites. It focuses on plates but another study dealing with preloaded shell is in progress. The objective is to study the influence of preload and impact energy on generated damage. To achieve this objective, a precharge device was designed. An experimental design was set to optimize the choice of test conditions. A home made drop tower device was used to perform impact. The damages generated were qualified and quantified by means of non-destructive techniques (NDT) and destructive techniques. Micrographic and deply techniques have been especially investigated.

2. Material and samples

The material used is an unidirectional carbon composite (UD T700) pre-impregnated with epoxy resin (M10R). Four rectangular plates of dimensions 450 mm ×500 mm and 5 mm in thickness were manufactured. The draping was carried out on a polished steel plate with a flatness of 0.1 mm m^{-1}. To limit preferential delamination [21,22], quasi-isotropic stacking sequence $([0/45/90/-45]_2)_S$ was chosen. Once draped, the plates were put under vacuum (−850 mbar) and inserted into an autoclave operating at 5 bar. The curing cycle is composed of two phases: 85 °C for 45 min and 120 °C for 60 min at heating and cooling rate of 2.6 °C m^{-1}.

Eight samples of size 100 mm × 230 mm were extracted from each plates. To avoid damage initiation associated with maintaining the samples in the preloading device, glass/epoxy tabs were glued. Moreover to improve the contact between the jaws of the preloading device and the sample, aluminum tabs were glued on those glass/epoxy tabs. Finally three drills 10.5 mm diameter were made at both ends to ensure load transmission. Fig. 1 represents a sample.

3. Experimental devices

To carry out experiments, the sample was placed in a preloading device and the impact was generated by a drop tower.

3.1. Preload device

A 60 kN device for imposing uniaxial preload was designed. This device, represented in Fig. 2(a), is composed of a rigid frame; two crossheads connection to the frame; two grips (each connected to one crosshead by a pivot connection); two threaded rods connecting each crosshead to the frame. One of the rod was equipped with a full-bridge strain gages to assess the applied preload as well as the stress in the rod during impact loading. Thanks to the pivot connection, the bending of the sample was allowed to avoid damage within the grips during impact. The impact took less than one minute after preloading to avoid accommodation of the specimen.

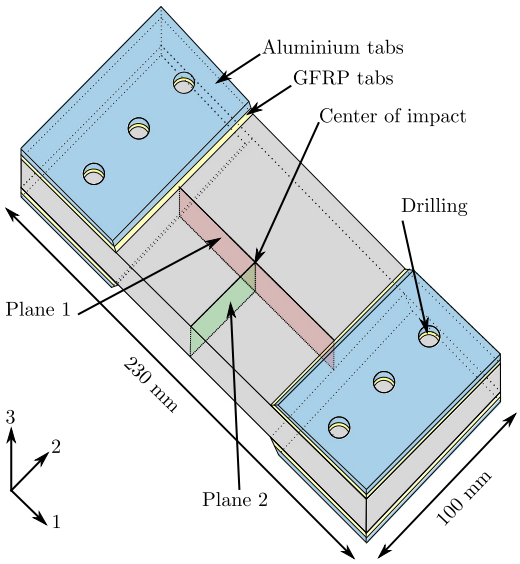

Fig. 1. Detail of a prepared sample with tabs and drilling, and the two planes for micrographic observations.

3.2. Home made drop tower

Drop tower device is commonly used to achieve impact loadings. This drop tower has two columns allowing the vertical translation of a mobile. These two columns are maintained by a rigid frame. An anti-rebound device allows a single impact of predefined incident energy. The drop tower, shown in Fig. 2(b), has a maximum capacity of 25 kg falling 2.80 m height. As a consequence, the maximum speed is about 7.4 m s^{-1} and the impact energy of about 700 J.

3.3. Instrumentation

During an impact test, the following values were recorded:

- The contact force between the impactor and the sample using a piezoelectric sensor (capacity 100 kN ± 1%).
- The position of the impactor (using a high speed camera clocked at 10000 image s^{-1} and a laser sensor).
  From these data, the impactor displacement and velocity can be easily derived.
- The tensile preload collected by the instrumented threaded rod.
- The angle of the rotation of the grip thanks to a high speed camera and images analysis.

4. Damage observation and quantification methods

After impacting a composite material, damages classically observed are: fiber breakage, delamination, debonding and matrix cracking (cf. Fig. 3). Damages are usually observed by non-destructive controls (like ultrasonic control) and micrographs (destructive). Few people use quantitative destructive technique to investigate damages. Some authors [23–25] use deply technique which consist on the destruction of the matrix by high temperature. This technique can be used to measure delamination and fiber breaks and can complete ultrasonic control. To observe and quantify them, three non destructive and destructive techniques were employed:

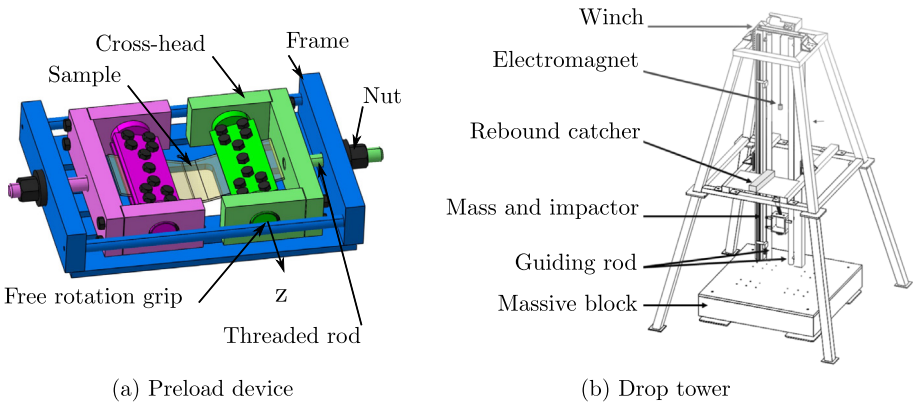

(a) Preload device (b) Drop tower

Fig. 2. Experimental devices.

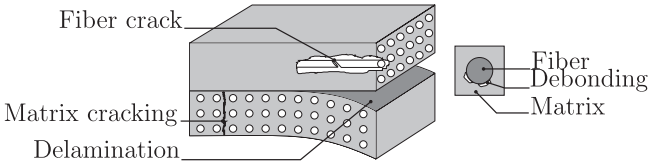

Fig. 3. Three kinds of damage in a composite.

- Non-destructive ultrasound to reveal and quantify delamination.
- Deply technique to reveal and quantify delamination and fiber breakage.
- Optical microscopy to reveal damage, but unable to allow quantification.

A description of these techniques is given in the following.

Non Destructive Technique (NDT) ultrasound investigations were performed with an OmniScan© MX-2, equipped with a 64 element sensor (transmitter/receiver) located on one line. The sensor was associated with an encoder to know its position on the sample and to allow a mapping of the plate. For a given sensor position, each element recorded an A-scan (reflected amplitude of wave), that is the reflection curve of the wave along a vertical below the element. All 64 A-scan constitute a S-scan which represent the material under the sensor. Fig. 4 shows a S-scan and the A-scan corresponding to the dashed vertical line. The encoder was set so that the S-scans were spaced from each other to 1 mm.

After recording, S-scans were combined with the ImageJ® image processing software to constitute a virtual volume. To observe and measure the delamination, this volume was observed along successive planes parallel to the folds, as shown in Fig. 5.

This technique has however some limitations:

Hidden zone: A delamination fully returns the ultrasonic signal emitted by the transmitter. Thus, the underlying delamination can not be detected. This implies that the deepest areas were not observable. That is why for delamination in the masked area, deply technique was used in order to complete the ultrasound technique.

Repeat echoes: A second echo (or sometimes several echoes) can be caused by delamination located in the upper half of the sample, as shown in Fig. 4. This echo is the result of an additional return of the ultrasonic signal. Nevertheless, these repetitions could easily be identified by observing the corresponding S-scan.

Deply technique: The deply technique, used by [23,25,24] consists of carbonizing matrix to reveal fiber breakage. The injection of a penetrant (ZnI_2) as in [25], causes a deposit on delaminated areas after carbonization of the matrix. This technique is of great help to quantify the delamination.

The deply technique protocol was as follows:

1. Holes 1 mm in diameter were performed along the thickness, over the damaged surface (after control by CND)
2. Zinc iodide (ZnI_2) diluted in a mixture of water and alcohol in equal proportions was injected into each of the holes with a syringe.
3. The samples were heated to 60 °C during 1 h to slowly evaporate the solvent.
4. The samples were heated to 440 °C during 2 h to carbonize the matrix and obtain the dry iodide and then zinc deposits along fibers.

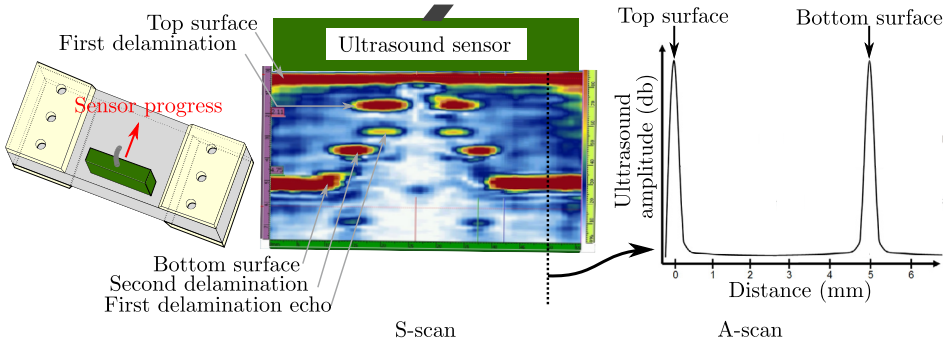

Fig. 4. Example of S-scan and A-scan recorded.

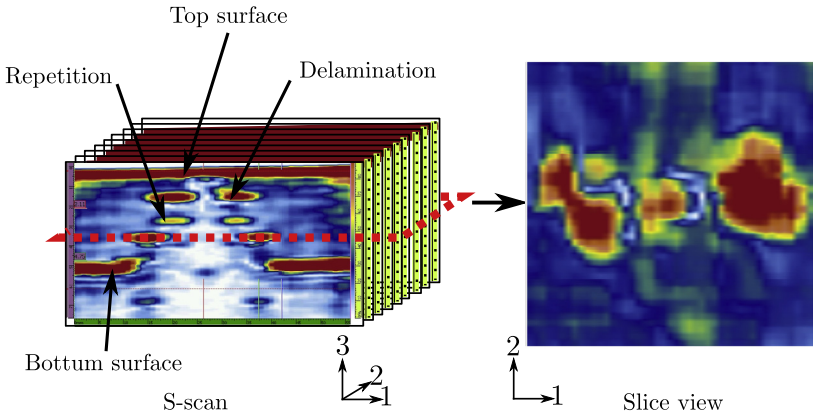

Fig. 5. Assembling of S-scan and slicing view.

5. Plies were removed one by one using an adhesive tape, and both sides of each ply were recorded.

Fig. 6 shows the same observation obtained by S-scan and deply technique. One can observe that the deposition of zinc iodide fits perfectly the delamination obtained by S-scan. Observations using both techniques were coupled to obtain better accuracy on the quantification of damage (especially the damage located at larger depth).

Optical micrographic: Two perpendicular planes (shown in Fig. 1) were polished to be observed with an optical microscope. This technique allows to control the type of damage revealed by the NDT. As the micrograph does not quantify the damage, it was not used thereafter.

5. Preliminary tests

Preliminary tests without preloading were realized to reach two objectives. The first one is to define the range of impact energy causing significant damage without destroying the sample and the second objective is to qualify the damage generated.

To minimize the number of tests to define such impact energy, a finite element analysis was first performed using the computer code Abaqus ©. The simulation reproduced a quasi-static indentation test with a hemispherical indenter 16 mm diameter (same dimension than the impactor). The composite plate was modeled by S4R elements (four-node shell element with reduced integration). The composite material constitutive law was modeled assuming an elastic behavior with constant properties recalled in Table 1. These properties were calculated with the rule of mixtures [26]. The orientation of the plies was modeled by the composite layups module. The boundary conditions of the plate were identical to those of the preloading system without preloading. To obtain damaged but not destroyed sample, a maximum stress in fiber direction was chosen as stopping criterion corresponding to the first fiber breakage (X_t=2400 MPa [27]).

Finite element calculations allowed to define the energy level required for the occurrence of a critical stress within one of the plies. To reach the critical stress X_t=2400 MPa an required energy of 62 J was needed.

Following the result of finite element calculation, an experiment with impact energy of 62 J was achieved on a sample (size 230 mm × 00 mm) attached to the preload device. A tension of 10 N was applied to adjust the bindings of the assembly.

Damage was observed by optical microscopy in planes marked schematically in Fig. 1. The micrographes are presented in Fig. 7 where the disc shows the position of the impactor. In the 0° direction (plane 1, Fig. 1), just beneath the impact point, a crater with fiber breaks was observed. Next to this crater zone, an important delamination was visible. Several 45° oblique matrix cracks were observed included in a cone crack. Many of them have lead to a delamination. The lower ply was peeled off because of large delamination.

In the 90° direction (plane 2, Fig. 1), crater zone was visible too. The upper plies were peeled off because of significant delamination. Three plies under, another important delamination was observed extending to the edge of the sample. Note that 45° oblique matrix cracks were not present in this plane because this plane was perpendicular to the bending direction.

Preliminary tests allow to identify the energy range used in the design of experiments as well as the qualification of damage.

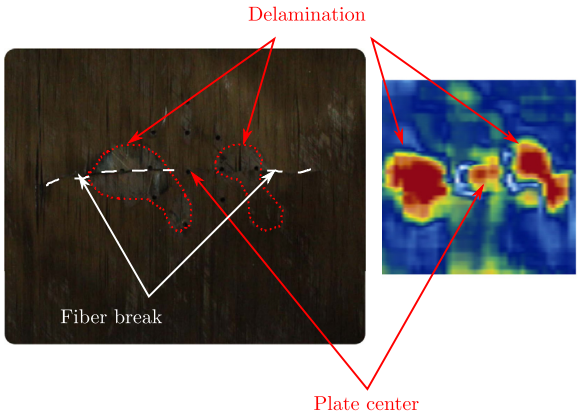

Fig. 6. Comparison of S-scan and deply images.

Table 1
Material properties of T700/epoxy ply.

Property	Value
Longitudinal stiffness, E_{11} (GPa)	130.0
Transverse stiffness, E_{22} (GPa)	9.5
Out-of-plane stiffness, E_{33} (GPa)	9.5
Poisson's ratio, $\nu_{12}, \nu_{13}, \nu_{23}$	0.3
Shear moduli, G_{12}, G_{13} (GPa)	3.5
Shear moduli, G_{23} (GPa)	5.0
Longitudinal tensile strength, X_t (MPa)	2400 [27]
Density (kg m^{-3})	1800

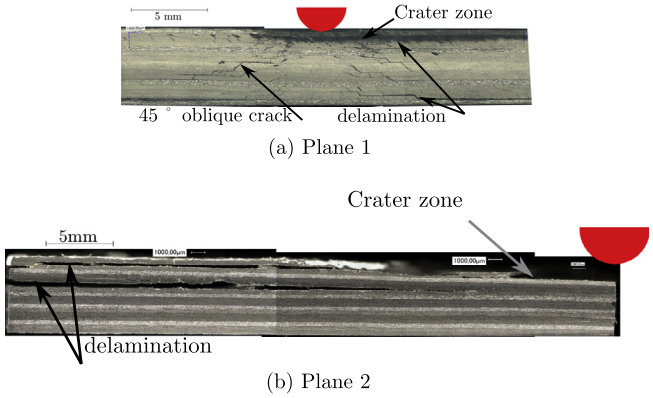

Fig. 7. Micrographs of sample impacted at 62 J.

6. Design of experiments

6.1. Choice of the design of experiments

A two-variable (X_1, X_2) design of experiments (DOE) was defined to optimize the choice of testing conditions and to obtain response surfaces with a limited number of tests. The desired responses were approached by response surface modeled with a second order polynomial (Eq. (1)). The variables X_1 and X_2 are standardized values of the two factors.

$$y = a_{11}X_1^2 + a_{22}X_2^2 + a_{12}X_1X_2 + a_1X_1 + a_2X_2 + a_0 \quad (1)$$

Doehlert design of experiments [28] was chosen due to the following advantages:

- Uniform distribution of the experimental points. The studied field is uniformity meshed. Thus, the interpolation of responses will be of consistent reliability.
- Extension of the matrix in the experimental field.The interest is to extend the field of study by adding a limited number of experiments.
- Increase the number of factor-study. If a new parameter must be studied, it is possible to add it and retain the experiments already performed.

6.2. The factors of the experimental design

The objective is to analyze the preloading effect on the plate damage for different impact energies. As a consequence, the two retained factors for the DOE were the value of the imposed preload and the impact energy.

6.2.1. Preload

In the literature, the preload is defined either by a strain [10,14,13,11,16] or by a percentage of the tensile strength [12]. The pre-strain was chosen for this study. Given the capacity of the preload device (60 kN) and the Young's modulus of the threaded rod material (40 GPa), the maximum value of the pre-strain is 3000 με.

6.2.2. The impact energy

The hemispherical impactor is in steel with a diameter of 16 mm. The impact energy is a parameter dependent on the mass and the velocity. But in this study, the relative influence of the mass or velocity is not analyzed. All the tests were carried out with an impact velocity between 4 m s^{-1} and 5 m s^{-1}.

The impact energy was expressed as a percentage of the reference energy defined by FEM modeling for unloaded sample (that is 62 J, *cf.* Section 5).

The two factor Doehlert design of experiments defined in the Table 2 is illustrated in Fig. 8.

6.3. Required responses

The required responses of the DOE are necessarily quantified responses. Most comparative responses with the literature are mainly the contact force and the maximum deflection of the plate. The energy dissipated during the impact is also an interesting response because it can be directly connected to the damage generated. additionally from both ultrasound technique and deply technique, the measures of sum of all delamination areas and the projected damage area give two quantified responses.

7. Results

As advised in [28], the test number 1, at the center of the experiment domain, was repeated 3 times to ensure the consistency and the repeatability. All the others experiments were repeated twice to ensure reproducibility, but also to be able to achieve a greater number of investigations to qualify and quantify the damage. To complete the investigations, test without preloading was performed (test point number 8). The overall results are shown in Table 3 (to simplify the readability only one result per test is reported).

7.1. Force vs time and force vs displacement diagrams

Fig. 9 represents the force vs time and the force vs displacement diagrams.

During the test, the angle of the rotation of the grip was measured thanks to a high speed camera. This measurement explains the shape of the force vs time diagrams where the vibration of the sample is perceptible (Fig. 9(a)). Upon contact, the rotation angle and the force increase until the point (a). From this point, the plate is leaking under the impactor. This causes a rapid increase on the rotational angle and a decrease of the force to point (b). At this point, the rotation angle is at its maximum, then the plate returns to the impactor, causing a diminution of the angle and the increase of force to a point (c). At this point, the contact force and the displacement of the impactor are at their maximum (Fig. 9(b)). The rebound of the impactor decreases the contact

Table 2
Design of experiments.

Num	X_1	X_2	Impact energy (% of 62 J)	Pre-strain (με)	Preload (kN)	Impact energy (J)
1	0	0	62.5	2000	40	39
2	1	0	100	2000	40	62
3	−1	0	25	2000	40	16
4	0.5	1	81.25	3000	60	50
5	−0.5	−1	43.75	1000	20	27
6	0.5	−1	81.25	1000	20	50
7	−0.5	1	43.75	3000	60	27
8	–	–	81.25	0	0	50

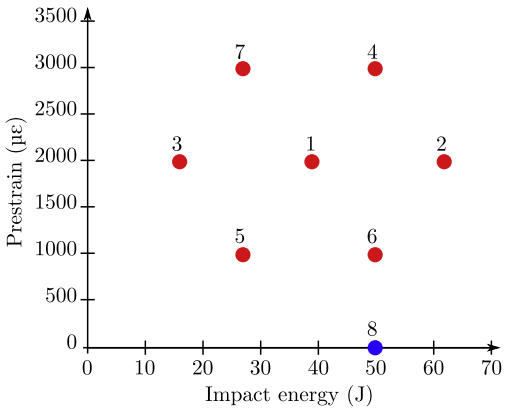

Fig. 8. Design of experiments (points 1–7), test without preload (point 8).

force. Each point can be identified on the force–displacement diagrams (Fig. 9(b)) On the curve of the angle versus time, we can see at the point (d) that the plate still oscillate.

7.1.1. Contact force (Eq. (2))

$$F = 1.430X_1^2 + 0.940X_2^2 + 0.826X_1X_2 + 4.262X_1 + 0.713X_2 + 7.610 \quad (2)$$

Fig. 10 represents the maximum force response surface as a function of the two parameters X_1(impact energy) and X_2(preload). This response was plotted in 3D and in isoline curve (2D). The second order polynomial approximation is given by Eq. (2). The coefficients of Eq. (2) as well as Fig. 10 show that the major contribution is the impact energy. In these curves, for constant impact energy, it's visible that the increasing preload rise the maximum contact force. These results are consistent with those of Chiu et al. [12] and Choi [11] who observed the same results for CFRP composite plates. At low impact energy, preload effect on maximum force value is insignificant; this phenomenon was also observed by Whittingham [14].

7.1.2. Deflection of the sample (Eq. (3))

$$D = -0.685X_1^2 + 0.975X_2^2 - 0.300X_1X_2 + 2.503X_1 - 1.594X_2 + 6.930 \quad (3)$$

The maximum deflection of the sample was determined from the position of the impactor. Fig. 11 represents the response surface for the maximum deflection. The deflection decreases as the preload increases for all impact energies. These results are consistent with those of Choi et al. [11] who observed that when the preload is lower, the deflection is upper. These results are confirmed with the Eq. (3), where the higher coefficient (X_2 coefficient) is negative.

7.1.3. Rate of energy dissipated during impact (RED) (Eq. (4))

$$\mathrm{RED} = -3.335X_1^2 - 8.255X_2^2 + 0.035X_1X_2 - 14.297X_1 + 7.448X_2 + 59.750 \quad (4)$$

Table 3
Table of measurements – DOE.

N	Impact energy ± 0.16 (J)	Prestrain (με)	Contact force ± 0.01 (kN)	Deflexion ± 0.03 (mm)	% Dissipated energy (%)	Projected damage area (mm²)	Cumul of delamination (mm²)	Fiber crack (mm)
1	35.7	2000	7.61	6.93	59.8	432	1150	6
1′	36.5	2000	9.48	6.69	58.7	490	1160	6.4
1″	36.2	2000	8.23	6.82	59.3	462	1146	6.7
2	56.4	2000	13.13	8.74	42.9	1072	2067	58
3	15.4	2000	4.95	3.75	69.9	0	0	0
4	48.0	3000	11.95	7.24	51.3	744	1954	2
5	26.1	1000	6.11	7.48	54.2	290	656	29
6	51.6	1000	10	10.26	38.3	1061	1550	78
7	26.3	3000	6.63	4.98	67.1	331	714	0

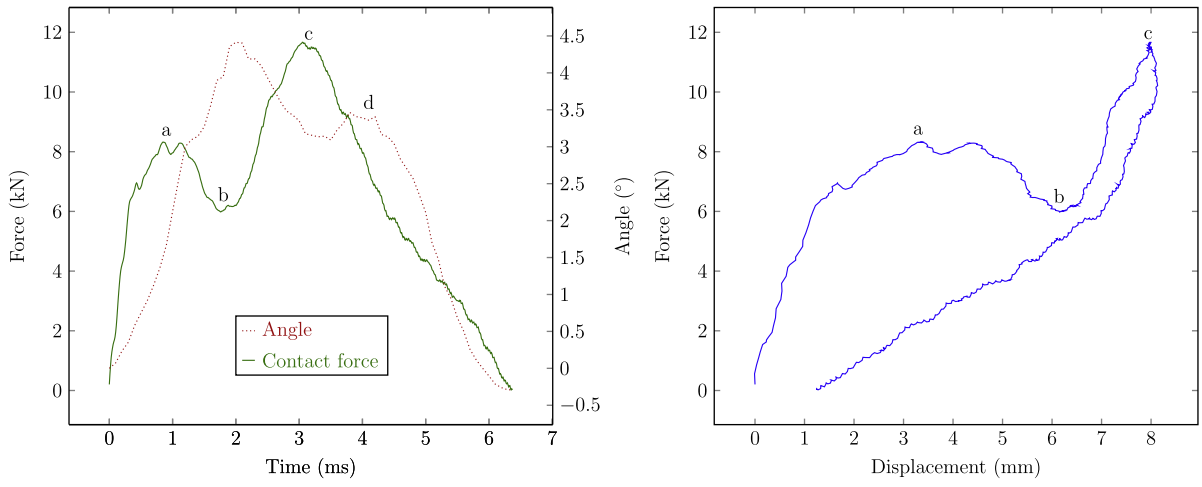

(a) Force vs time and rotation vs time

(b) Force vs displacement

Fig. 9. Diagrams for the sample number 4 in the DOE.

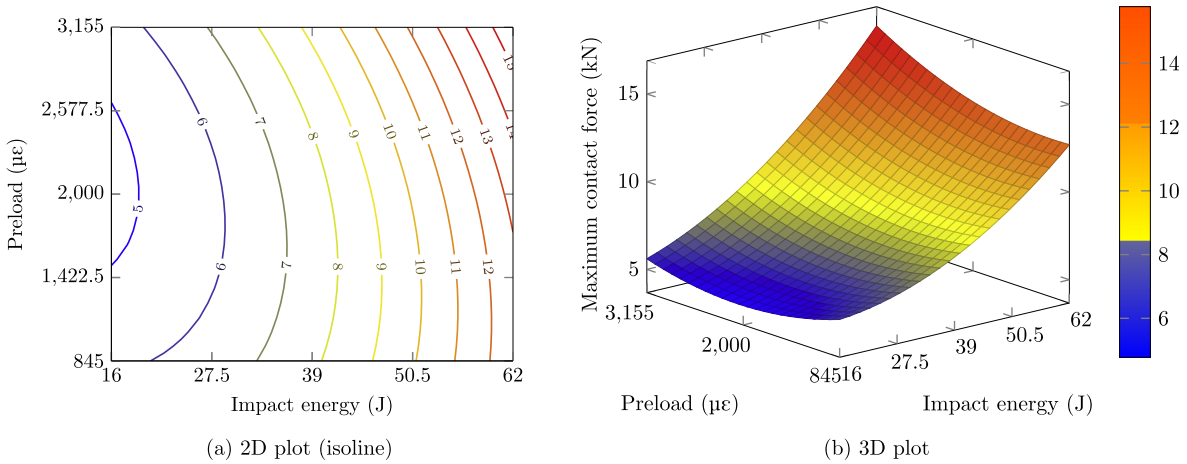

(a) 2D plot (isoline) (b) 3D plot

Fig. 10. DOE reconstruction of maximum contact force (kN) depending on the impact energy and preload.

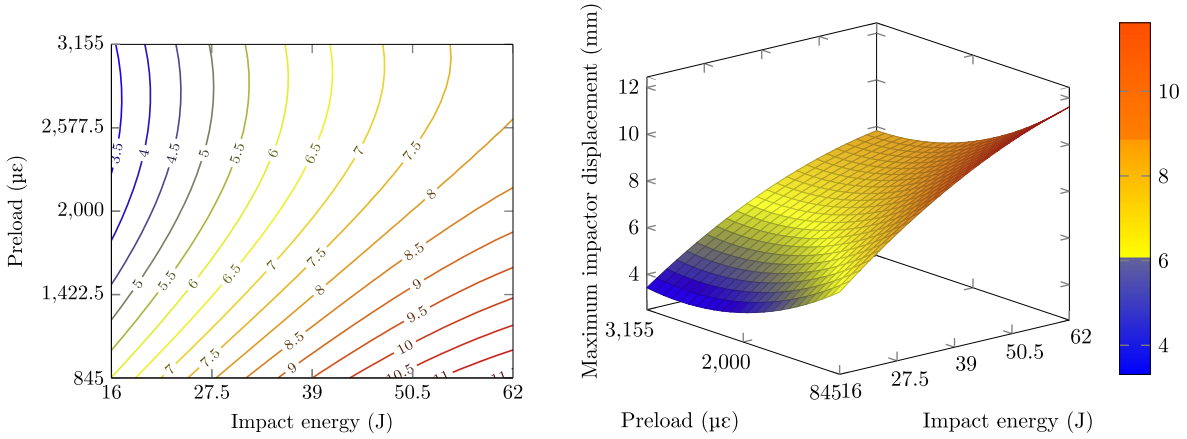

(a) 2D plot (isoline) (b) 3D plot

Fig. 11. DOE reconstruction of maximum deflection (mm) depending on the impact energy and preload.

The energy dissipated during impact was estimated as the kinetic energy lost by the impactor during the impact. This energy is the difference between the kinetic energy of the impactor before and after impact. Energy dissipation rate was defined as the ratio of the energy dissipated on the incident energy of the impactor. Fig. 12 represents the energy dissipation rate response surface. This rate was highest for high preload and low impact energy. This rate was mainly directed by the X_1 coefficient and show that this rate decrease as impact energy increase. For constant impact energy, if preloading increases, the absorbed energy increases (confirmed by the X_2 coefficient of Eq. (4)).

7.2. Damages

7.2.1. Fiber breakage

Fiber breaks were observed using the deply technique. Observations show that the fiber breaking occurs only into the first two plies from the impacted face. These failures are due to buckling of the sample during the impact. Such fiber breaks occur at low preload and high impact energies.

7.2.2. Projected damaged area (PDA) (Fig. 13, Eq. (5))

$$PDA = 104.00X_1^2 + 198.012X_2^2 - 206.697X_1X_2 + 554.667X_1 - 79.677X_2 + 432.00 \quad (5)$$

The damaged area considered is the projected delamination area obtained from c-scan investigations. This area remains approximately constant for low impact energy and increases as impact energy is raised, and prestrain is reduced. On the contrary, Choi et al. [11] observed that damaged area increased with preload uniaxial tension. This difference in evolution is probably due to the boundary conditions. Indeed, the rotation at the jaws is not permitted in the Choi et al. [11] device. The rotation at the jaws can be more representative of large plate where the bridles are far from the impact zone.

7.2.3. Sum of delamination area (SDA) (Fig. 14, Eq. (6))

$$SDA = -116.48X_1^2 + 130.781X_2^2 + 199.907X_1X_2 + 1044.58X_1 + 133.58X_2 + 1150.08 \quad (6)$$

The cumulative delamination is the sum of delamination areas observed on all interfaces of the sample. Each area is localized using both c-scan and deply technique; the last makes it possible to quantify that area. This sum is maximum for high impact energy and high preload. The preload tends to increase the total area of delaminations.

As for damaged area, cumulative delamination remains constant and very low for low impact energy and increases versus impact energy. Nevertheless, its development is promoted by high prestrain.

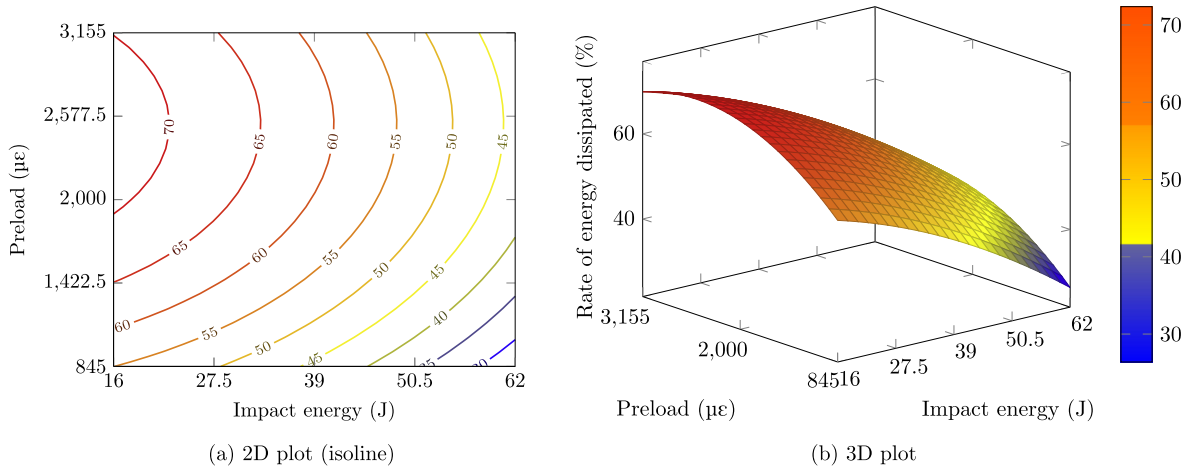

Fig. 12. DOE reconstruction of rate of energy dissipated during impact as a function of the impact energy and preload.

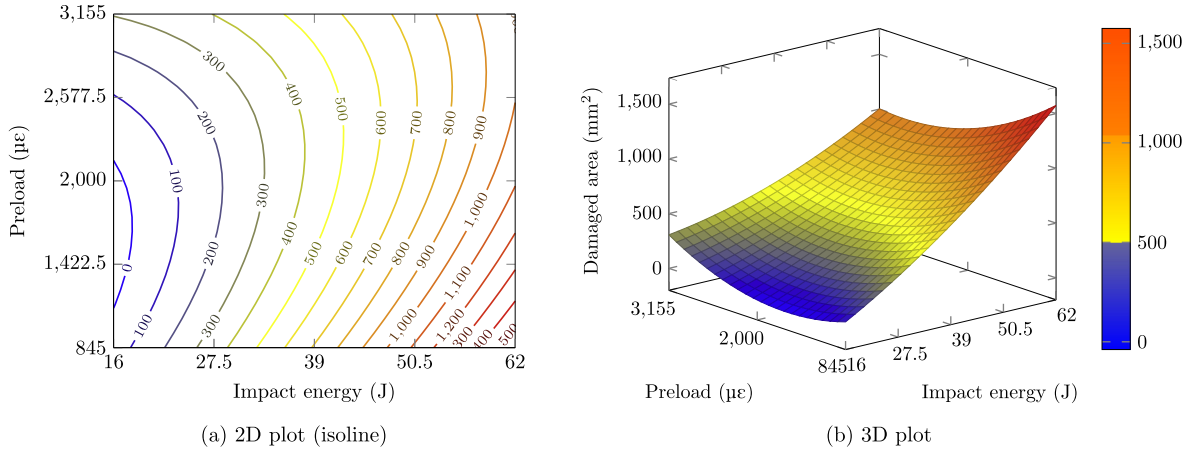

Fig. 13. DOE reconstruction of projected damaged area (mm^2) depending on the impact energy and preload.

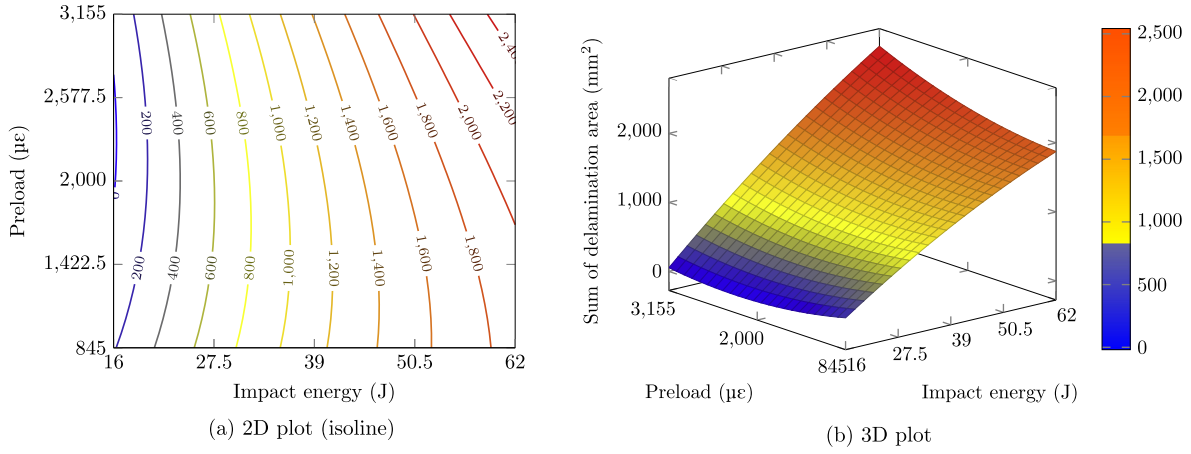

Fig. 14. DOE reconstruction of sum of delamination area (mm^2) depending on the impact energy and preload.

If we compare the projected damage area equation and the sum of delamination area, the major difference is for the X_2 coefficient. It was positive for the SDA and negative for PDA. That confirms the increase of the SDA and the decrease of the PDA when the preload increases.

7.3. Test without prestress

Two tests were performed at the impact energy of 50 J: the first one is performed at the preload of 3000 με (impact number 4), the second one at the preload of 1000 με (impact number 6). A 50 J

Table 4
Table of measurements – same impact energy.

N	Impact energy (J)	Prestrain (με)	Contact force (kN)	Deflexion (mm)	% Dissipated energy (%)	Projected damage area (mm^2)	Cumul of delamination (mm^2)	Fiber crack (mm)
4	48.0	3000	11.95	7.24	51.3	744	1954	2
6	51.6	1000	10	10.26	38.3	1061	1550	78
8	49.5	0	7.24	12.5	38.5	1159	1374	114

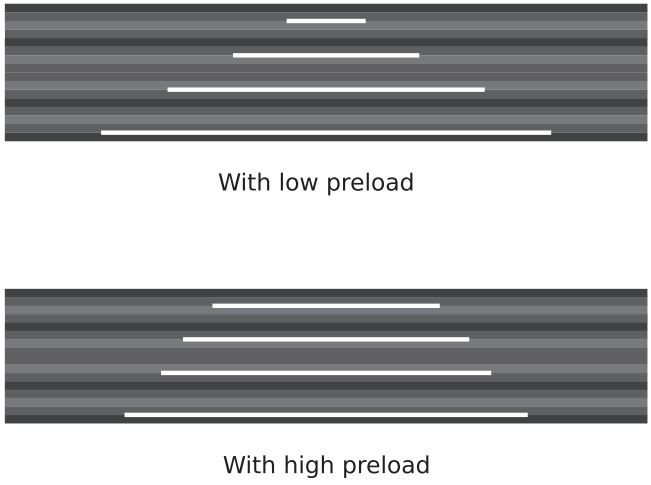

Fig. 15. Scheme of distribution and amount of delamination depending on preload for a given impact energy.

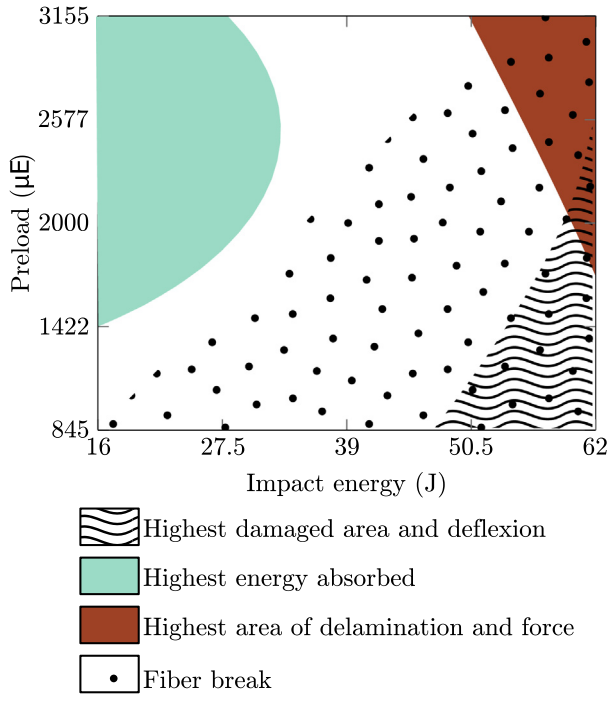

Fig. 16. Regions of interest depending on the impact energy and preload.

impact test was performed on unloaded specimen to check the effect of different preload values. This test is performed with the same preload device. A tension of 10 N was applied to adjust the bindings of the assembly. Table 4 compares results of the three 50 J impact tests.

These results confirm the hypothesis shown in previous section. All the responses agree with the response surface trend and particularly the two major results are confirmed:

— Damage area increases when the preloading decreases
— Sum of delamination increases when the preloading increases

All the results of the unpreload test are in agreement with previous test.

8. Discussion

The main influence of sample preloading is increasing the sample stiffness. This explains the increase of impact contact force and the decrease of the sample deflection. The observed fiber breakage are induced by the largest deflection. So, increasing the preload leads to a decrease of fiber breakage caused by buckling.

Due to the stacking sequence, initial preloading induces shearing state between plies with different orientations. The sum of this shear and the shear due to the impact promote the apparition of delamination. That's why for a given impact energy, the cumulative area of delamination increases with the preload despite the projected area decreases. Fig. 15 illustrates the distribution and amount of delamination. Moreover, this may explain that the energy dissipated is greater when the preload is high despite that there is no fiber breakage for high preloads (Table 4).

9. Conclusion

A preloading device has been designed to allow a good representation of loading cases found for structural parts. Indeed, the rotation of the plates gives boundary conditions representative of structural reality.

Low velocity impacts on thick laminated composite plates CFRP with tensile preload were studied. Experimental investigation with several levels of preload up to 3000 με have been carried out. The contact force, the deflection of the sample and the rate of dissipated energy were measured. Original methods (deply-technique and ultrasonic control) were used to observe, locate and quantify damages. The major results to be underlined are:

- The cumulative area of delamination is increased when preload is applied.
- The projected damaged area is reduced when a preload is applied.
- The maximum contact force varies in the same way as the preload.
- At fixed impact energy, the maximum displacement of the impactor decreases as the preload increases. The preload increases the stiffness of the sample.
- The rate of energy absorbed during the impact is greater for high preload and a low impact energy.

Fig. 16 shows the advantage of different configurations (impact energy/preloading). For example, in shock protection, composite structures could absorb more energy if they are preloaded (In blue

on the picture), or preloading can be used to reduce fiber breaks by limiting the deflection of the structure (Zone without dot).

Future work will concern the low velocity impacts on wound CFRP pipes under pressure. The influence of stratification, thickness and pressure loading on damages will be especially addressed.

Acknowledgments

The authors gratefully acknowledge the support of "Agence Nationale de la Recherche" and especially the collaborators of "Toledo".

References

[1] Freitas MD, Silva A, Reis L. Numerical evaluation of failure mechanisms on composite specimens subjected to impact loading. Compos Part B: Eng 2000;31:199–207.
[2] Kadlec M. Failure mechanism and strain fields on a carbon/epoxy composite subjected to compression after impact. Eng Mech 2011:107–18.
[3] Tita V, de Carvalho J, Vandepitte D. Failure analysis of low velocity impact on thin composite laminates: experimental and numerical approaches. Compos Struct 2008;83(4):413–28.
[4] Abrate S. Impact on laminated composite structures. Appl Mech Rev 1991;44(4):155–90.
[5] Abrate S. Impact on laminated composite structures: recent advances. Appl Mech Rev 1994;47(5):517–44.
[6] Abrate S. Impact on composite structures. Cambridge University Press; 2005.
[7] Cantwell W, Morton J. The impact resistance of composite materials a review. Composites 1991;22(5):347–62.
[8] Richardson M, Wisheart M. Review of low-velocity impact properties of composite materials. Compos Part A: Appl Sci Manuf 1996;27(12):1123–31.
[9] Saghafi H, Minak G, Zucchelli A. Effect of preload on the impact response of curved composite panels. Compos Part B: Eng 2014;60:74–81.
[10] Robb MD, Arnold WS, Marshall I. The damage tolerance of GRP laminates under biaxial prestress. Compos Struct 1995;32:141–9.
[11] Choi I-H, Kim I-G, Ahn S-M, Yeom C-H. Analytical and experimental studies on the low-velocity impact response and damage of composite laminates under in-plane loads with structural damping effects. Compos Sci Technol 2010;70(10):1513–22.
[12] Chiu S-T, Liou Y-Y, Chang Y-C, Ong C-L. Low velocity impact behavior of prestressed composite laminates. Mater Chem Phys 1997;47(2-3):268–72.
[13] Mitrevski T, Marshall I, Thomson R, Jones R. Low-velocity impacts on preloaded GFRP specimens with various impactor shapes. Compos Struct 2006;76(3):209–17.
[14] Whittingham B, Marshall I, Mitrevski T, Jones R. The response of composite structures with pre-stress subject to low velocity impact damage. Compos Struct 2004;66(1-4):685–98.
[15] Ghelli D, Minak G. Numerical analysis of the effect of membrane preloads on the low-speed impact response of composite laminates. Mech Compos Mater 2010;46(3):299–316.
[16] Kulkarni M, Goel R, Naik N. Effect of back pressure on impact and compression-after-impact characteristics of composites. Compos Struct 2011;93(2):944–51.
[17] Wardle B, Lagace P. Behavior of composite shells under transverse impact and quasi-static loading. AIAA J 1998;36(6):1065–73.
[18] Heimbs S, Bergmann T, Schueler D, Toso-Pentecôte N. High velocity impact on preloaded composite plates. Compos Struct 2014(0):158–68.
[19] García-Castillo SK, Sánchez-Sáez S, Barbero E, Navarro C. Response of preloaded laminate composite plates subject to high velocity impact. J Phys IV (Proc) 2006;134:1257–63.
[20] García-Castillo S, Sánchez-Sáez S, López-Puente J, Barbero E, Navarro C. Impact behaviour of preloaded glass/polyester woven plates. Compos Sci Technol 2009;69(6):711–7.
[21] Fuoss E, Straznicky P, Poon C. Effects of stacking sequence on the impact resistance in composite laminates – part 1: parametric study. Compos Struct 1998;98:67–77.
[22] Fuoss E, Straznicky P, Poon C. Effects of stacking sequence on the impact resistance in composite laminates – part 2: prediction method. Compos Struct 1998:177–86.
[23] Freeman S. Characterization of lamina and interlaminar damage in graphite/epoxy composites by the deply technique. Am Soc Testing Des 1982;32:50–62.
[24] Breen C, Guild F, Pavier M. Impact damage to thick carbon fibre reinforced plastic composite laminates. J Mater Sc 2006;41(20):6718–24.
[25] Pavier M, Clarke M. Experimental techniques for the investigation of the effects of impact damage on carbon–fibre composites. Compos Sci Technol 1995;55(2):157–69.
[26] Berthelot J-M. Matériaux composites. Comportement mécanique et analyse des structures. Éditions Tec& Doc; 1999 [in french].
[27] Kim C-U, Hong C-S, Kim C-G, Kim J-Y. Optimal design of filament wound type 3 tanks under internal pressure using a modified genetic algorithm. Compos Struct 2005;71(1):16–25.
[28] Droesbeke J, Saporta G, Fine J, Société de statistique de France. Plans d'expériences: applications à l'entreprise. Technip; 1997 [in french].